

Growth and Characterization of SbSI Ferroelectric Thin Film

Matthew D. Felder

University Undergraduate Research Fellow, 1994-95

Texas A&M University

Department of Electrical Engineering

APPROVED

Undergraduate Advisor



Exec. Dir., Honors Program

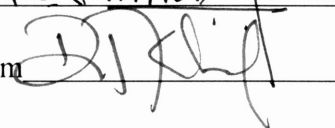


## Table of Contents

|   |     |
|---|-----|
| List of Illustrations                                   | ii  |
| Glossary  | iii |
| I. Introduction   | 1   |
| Background to the Properties of Ferroelectric Materials |     |
| Ferroelectric Thin Films                                |     |
| Non-Volatile Memory Applications                        |     |
| Volatile Memory Applications                            |     |
| Infra-red Detector Applications                         |     |
| Properties of Antimony Sulfo-Iodide                     |     |
| II. Experimental Procedure                              | 9   |
| Growth of SbSI Thin Film                                | 9   |
| Substrates  |     |
| Physical Vapor Transport                                |     |
| Buffer Layer of $\text{Sb}_2\text{S}_3$                 |     |
| Pre-annealing   |     |
| Characterization of SbSI Thin Film                      | 12  |
| Scanning Electron Microscopy                            |     |
| Electron Dispersion Spectroscopy                        |     |
| X-Ray Diffraction                                       |     |
| Electrical Characterization                             |     |
| III. Results  | 15  |
| First Growth  |     |
| Buffer Layers   |     |
| Pre-annealing   |     |
| IV. Work to be Completed                                | 19  |
| Acknowledgments   | 20  |
| References Cited  | 21  |
| Works Consulted   | 22  |

## List of Illustrations

- Figure 1. Ferroelectric material sub-grouping
- Figure 2. Unit cell of a perovskite ferroelectric material
- Figure 3. Hysteresis loop for a ferroelectric material
- Figure 4. Transition from the ferroelectric phase to the paraelectric phase
- Figure 5. Dielectric permittivity of a ferroelectric material
- Figure 6. Crystal Structure of SbSI
- Figure 7. SbSI single crystal dielectric constant
- Figure 8. SbSI thick film (20  $\mu\text{m}$ ) dielectric constant
- Figure 9. Closed-tube growth mechanism
- Figure 10. Electrical Characterization Setup
- Figure 11. SEM of an SbSI film grown on an annealed platinized silicon substrate
- Figure 12. XRD of an SbSI film grown on an annealed platinized silicon substrate
- Figure 13. SEM of an SbSI film grown with a sulfide buffer layer
- Figure 14. XRD of an SbSI film grown with a sulfide buffer layer
- Figure 15. XRD of an SbSI film grown with a 250°C pre-annealed sulfide buffer layer
- Figure 16. XRD of an SbSI film grown with a 300°C pre-annealed sulfide buffer layer

## Glossary

|                                |  |
|--------------------------------|--|
| <b>buffer layer</b>            | temporary intermediate deposition layer used to lower the critical energy for nucleation   |
| <b>Curie point</b>             | transition temperature where a ferroelectric material enters the paraelectric phase; temperature where the spontaneous polarization is zero              |
| <b>Curie-Weiss temperature</b> | temperature that determines ferroelectric material dielectric permittivity in the paraelectric phase   |
| <b>dielectric</b>              | material that acts as an insulator   |
| <b>DRAM</b>                    | Dynamic Read Only Memory; a volatile memory that is the cheapest semiconductor memory, made from a simple one-transistor gate design                     |
| <b>EDS</b>                     | Energy Dispersive Spectroscopy, used to determine the chemical composition (stoichiometry) of a sample   |
| <b>EEPROM</b>                  | Electrically Erasable, Programmable Read Only Memory; fastest non-volatile memory  |
| <b>ferroelectric</b>           | polar material that has a reversible spontaneous polarization  |
| <b>non-volatile memory</b>     | memory that does not require power to maintain data  |
| <b>paraelectric phase</b>      | phase of a ferroelectric material that is characterized by a zero spontaneous polarization and a high dielectric permittivity; begins at the Curie point |
| <b>polar material</b>          | dielectric that can be spontaneously polarized by an electric field  |
| <b>post-annealing</b>          | heating the final film to improve stoichiometry or orientation   |
| <b>pre-annealing</b>           | heating the buffer layer to improve its crystallinity which can improve the density and affect orientation of the final film                             |
| <b>pyro-optic effect</b>       | refractive index is altered by local temperature variations caused by infrared radiation   |
| <b>remanent polarization</b>   | magnitude of polarization in the absence of an electric field  |



|                                 |   |
|---------------------------------|---|
| <b>SEM</b>                      | Scanning Electron Microscopy, used to view the surface of a material with some field of depth                 |
| <b>single crystal</b>           | periodic arrangement of atoms (unit cells) grown in three dimensions  |
| <b>spontaneous polarization</b> | polarization induced by the internal field of a polar material  |
| <b>SRAM</b>                     | Static Read Only Memory   |
| <b>stoichiometry</b>            | the chemical composition of a substance   |
| <b>substrate</b>                | material being deposited onto   |
| <b>switching voltage</b>        | voltage required to produce an electric field capable of reversing the ferroelectric spontaneous polarization |
| <b>unit cell</b>                | smallest atomic periodicity of a lattice that makes up the entire structure of a single crystal               |
| <b>XRD</b>                      | X-Ray Diffraction, uses Bragg Law to determine the crystal structure and orientation                          |

# I. Introduction

## Background to the Properties of Ferroelectric Materials

Ferroelectric materials are a subgroup of each of the groups shown in Figure 1. Each group has characteristic properties that lend to their use in a variety of applications. Since, ferroelectrics belong to all of the groups, they possess all of the properties and can be used for a wide range of applications.

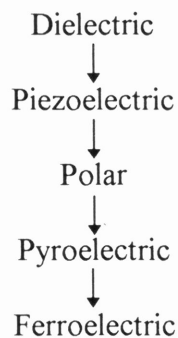


**Figure 1.** Ferroelectric material sub-grouping.

Dielectric materials are commonly known as insulators; they are non-conducting. All dielectrics can be polarized by placing them in an electric field.

Piezoelectric materials convert pressure into a polarization. The most common piezoelectric material is the quartz crystal, used in most modern clocks.

Polar materials are dielectrics that maintain a spontaneous polarization without the presence of an electric field. The spontaneous polarization is caused by asymmetry of the basic crystal cell. A perovskite ferroelectric crystal cell is shown in Figure 2. An electric field would displace the center cation, causing the polarization to develop.

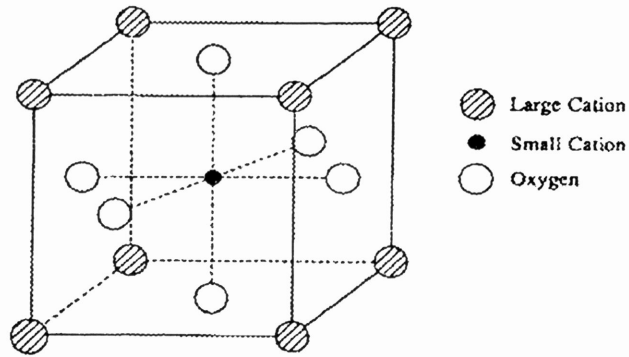


**Figure 2.** Unit cell of a perovskite ferroelectric material. [1]

Pyroelectric materials produce thermally induced current when subjected to a thermal gradient. This property is one basis for the development of thermal detectors.

A ferroelectric material is a polar material whose spontaneous polarization can be reversed with an applied electric field. The reversible spontaneous polarization gives ferroelectric materials the hysteresis loop shown in Figure 3.

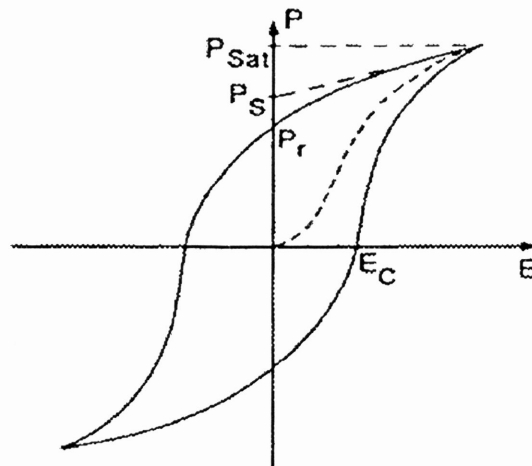


**Figure 3.** Hysteresis loop for a ferroelectric material. [1]

Ferroelectric materials only display ferroelectric properties when they are below the Curie temperature. When a ferroelectric material is cooled below the transition temperature (i.e. the Curie temperature) in the presence of an electric field, regions of

aligned electric dipoles form. This is called “poling” the material. The spontaneous polarization is caused by the collective effort of aligned electrical dipoles or domains.  $P_{\text{sat}}$  corresponds to the maximum alignment of these domains. Since this is a function of the quality of the material, single crystals have the largest values of  $P_{\text{sat}}$ . When the electric field is removed, the polarization relaxes to  $P_r$ , the remanent polarization.  $E_c$  is the coercive electric field necessary to reduce the spontaneous polarization to zero.

Above the Curie temperature the unit cell of the material changes from a non-centro-symmetric configuration to a centro-symmetric structure. This state is called the paraelectric phase. The material then no longer exhibits a spontaneous polarization (see Figure 4).

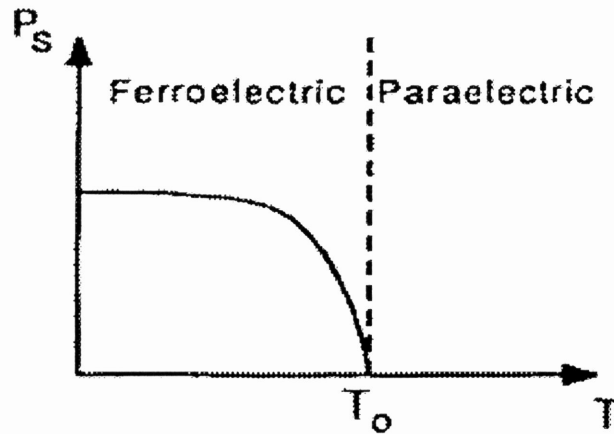


**Figure 4.** Transition from the ferroelectric phase to the paraelectric phase. [1]

Another significant property of ferroelectric materials is a very high dielectric constant that is temperature dependent. The dielectric permittivity in the paraelectric phase exhibits Curie-Weiss behavior:

$$\varepsilon = \frac{C}{(T - T_0)} \quad (1)$$

where  $T_0$  is the Curie-Weiss temperature. The Curie-Weiss temperature is a constant value that is characteristic of the particular ferroelectric material.  $C$  is a constant that is dependent on the type and quality of the ferroelectric crystal. A typical graph of the dielectric permittivity as a function of temperature is shown in Figure 5.

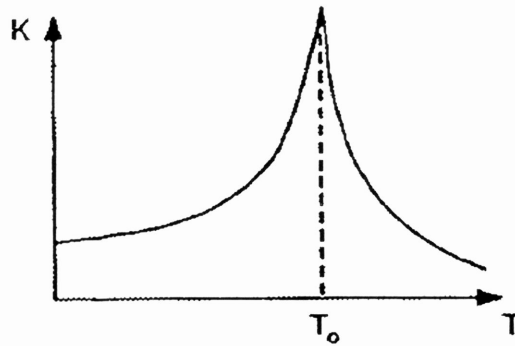


**Figure 5.** Dielectric permittivity of a ferroelectric material. [1]

### Ferroelectric Thin Films

Ferroelectric substances can be grown as single crystals, ceramics, crystalline films, and amorphous films. Single crystals have the fewest imperfections and the best alignment of domains. Therefore, single crystals produce the highest values of spontaneous polarization and dielectric constant. Thin films can be produced as two dimensional single crystals using epitaxial growth. There are many methods of making thin films (these will be described later), but usually it is desired to produce the most crystalline film possible. Ceramics and amorphous films are much easier to produce, but the film quality is sacrificed.

Thickness is another factor of film growth. Many applications of ferroelectrics call for the thinnest film possible. The advantages of thin films are: 1) ability to integrate films with semiconductor structures for novel applications, 2) ability to create large capacitances, and 3) low switching voltages. All of these are important factors in computer memory design.

### Non-Volatile Memory Applications

Ferroelectric materials can be implemented in a non-volatile memory cell by taking advantage of the reversible spontaneous polarization. Polarization is a measurable electrical value defined as:

$$P = \frac{q}{A} \quad (2)$$

where  $q$  is the charge at the electrodes and  $A$  is the electroded area. In the ferroelectric phase, a poled material will retain a remanent polarization in the absence of an electric field. This is the inherent non-volatility of the material; the polarized value will remain intact even during a power failure. Since ferroelectric memory uses a polarization instead of a stored charge, there is no leakage current, so no refresh cycles are needed and no battery backup is required. The reversible polarization of ferroelectrics as seen in the hysteresis loop (see Figure 3) allows binary data to be stored. Also, the data can be easily updated (random access) unlike an EEPROM.

## Volatile Memory Applications

Ferroelectric materials are seriously being considered in order to meet the specifications for the next generation of DRAM cells. The next few formulas apply to dynamic memory implementation. All materials have a characteristic dielectric permittivity:

$$\epsilon = k\epsilon_0 \quad (3)$$

where  $\epsilon_0$  is the permittivity of free space (a constant) and  $k$  is the relative permittivity.

Dynamic memories are made with a switch (a transistor) and a capacitor that holds a charge (data), but needs to be frequently refreshed (recharged) due to leakage currents that drain the charge. The capacitance of a dielectric material is:

$$C = \frac{\epsilon A}{d} \quad (4)$$

where  $A$  is the electroded area and  $d$  is the thickness of the dielectric material. To increase the density of memory cells in DRAM, it is desired to reduce the area of the dielectric. However, the capacitance has to meet a certain specification to store an adequate, reliable charge. A reduction in the thickness of the dielectric will compensate for the reduction in area.

The cell area and thickness of the dielectric material have been stretched to the process limits in the design of the latest generation of DRAM. Intel mass produced the 4kb DRAM in 1972. Every three years a new generation of DRAM was developed that quadrupled the capacity of the previous generation. These improvements were made mainly through reduction in feature size. Following the memory generation trend, in 1993 the 64Mb DRAM was introduced. The 16Mb and 64Mb DRAMs required the use of

stacked or trench capacitors to achieve the necessary density of memory cells. This is an expensive method for the fabrication of the DRAMs. Future generations of DRAM (256Mb and higher) will require a new capacitive material with a higher dielectric constant. If the dielectric constant is high enough, it might be possible to eliminate stacked or trenched capacitors, thereby lowering the fabrication cost.

The high dielectric constant of ferroelectric materials makes them an ideal candidate for this new generation of DRAM cells. Figure 5 shows that the dielectric permittivity in a ferroelectric material is strongly dependent on the temperature. Although the peak dielectric permittivity is at the Curie temperature, for reliability it is desired to operate well above the Curie temperature, in the paraelectric phase.

#### Infra-red Detector Applications

SbSI not only has ferroelectric properties, it also exhibits the pyro-optic effect. The pyro-optic effect causes the refractive index of the material to change with local temperature variations caused by infra-red radiation. An infra-red detector can be made by focusing the incident infra-red image onto one side of the SbSI film. A light beam is projected onto the other side of the film, and the reflected beam is picked up by a sensor array. The sensor can then construct an infra-red image from the reflected beam, that were caused by changes in reflectance of the SbSI film.



## Properties of Antimony Sulfo-Iodide (SbSI)

Ferroelectric SbSI has many interesting properties, some of which are attractive to implementations in computer memory or infra-red detectors. SbSI has a high growth rate along the c-axis and forms needles (shown in Figure 6). The needles are held together by Van der Waals bonds.

These needle structures and large differences in vapor pressure of antimony, sulfur, and

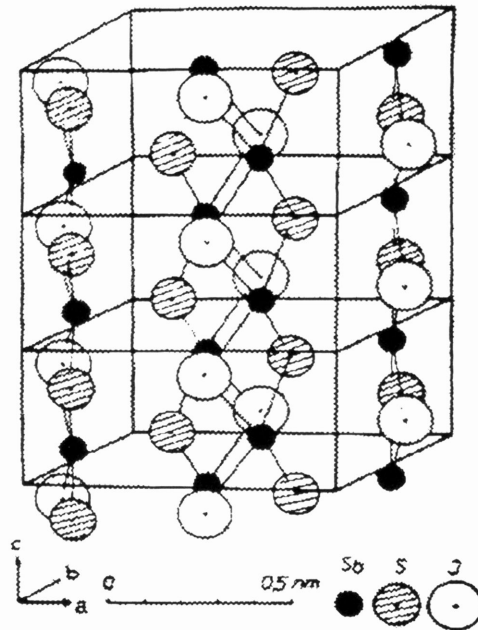


**Figure 6.** Crystal structure of SbSI. [2]

iodine complicate the controlled growth of an SbSI thin film. It is difficult to grow SbSI with the needles in the desired orientation. The highest polarization and dielectric constant (for computer memory applications) are realized with c-axis oriented crystals. Optical properties (for infra-red detection) are better with the c-axis parallel to the substrate.

The large differences in vapor pressure make it hard to produce a stoichiometric film. Past SbSI stoichiometric films have been produced by annealing the films in a sulfur, iodine, or argon atmospheres [3] [4]. Post-deposition annealing to improve stoichiometry can be a complicated and sensitive process. It is preferred to find a growth mechanism that produces stoichiometric SbSI.

The Curie temperature of SbSI is 21 °C, the highest Curie temperature for the V-VI-VII class compounds. The dielectric constant of SbSI is shown in Figure 7 and Figure

8. The dielectric constant of SbSI is in the desired range for applications in computer memory.

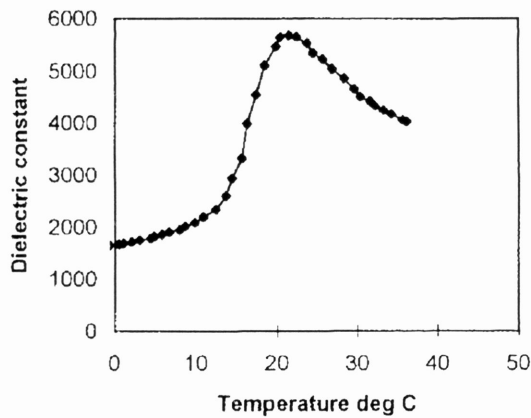


Figure 7. SbSI single crystal dielectric constant.

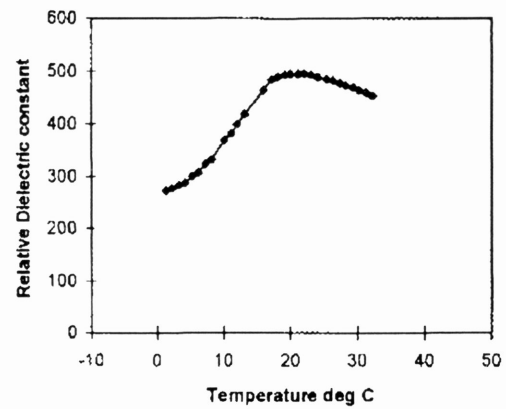


Figure 8. SbSI thick film (20µm) dielectric constant.

## II. EXPERIMENTAL PROCEDURE

### Growth of SbSI Thin Film

#### Substrates

The first problem to face when growing a high dielectric constant film is choosing a suitable substrate. The substrate will support the film, and if its lattice constants are properly matched, epitaxial films can be grown. The metallized substrate will function as the bottom electrode of the film, and the top electrode will be deposited onto the film by gold sputtering or thermal evaporation. The metal coating on the substrate must not be subject to oxidation. Oxidation of the substrate will produce a low dielectric constant material in series with the high dielectric constant material that results in a very poor

capacitance. Platinized silicon is an option, however an intermediate Tantalum layer must be used in order to avoid producing PtSi at 370 °C. Pt-Ta-SiO<sub>2</sub>-Si substrates were used for all experiments to perform electrical characterization. Films were also grown on MgO and Al<sub>2</sub>O<sub>3</sub> (sapphire) transparent substrates for optical applications.

### Physical Vapor Transport

The second problem to overcome with SbSI was the great differences in vapor pressure for Sb, S, and I. The SbSI films were grown in a closed, evacuated tube (Figure 9). This provided a more stoichiometric film than growth by open-system evaporation methods. Powder form of SbSI (the charge) was pelletized and placed in the end of a quartz ampoule. The substrate was placed on the end of a quartz bead with a thermal epoxy. The quartz bead was placed into the ampoule at a given distance (determined by experiment), and the ampoule was evacuated to approximately 10<sup>-6</sup> torr. The ampoule was then sealed by melting the ampoule around the bead with an oxy-acetylene torch. To avoid heating the substrate during sealing a second sealing bead was used that was placed further back from the bead holding the substrate. After sealing, the ampoule was placed into a two-zone furnace where the films were deposited using the temperature scheme shown in Figure 9. During the growth, the SbSI charge would sublime, vapor transport would occur, and SbSI would deposit onto the substrate. The samples were removed by snap-cutting the ampoule.

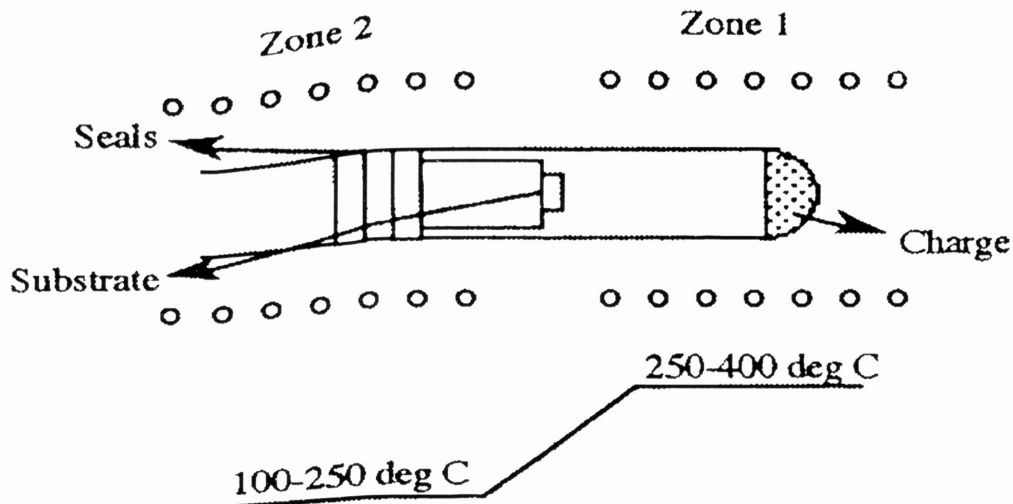


Figure 9. Closed-tube growth mechanism.

### Buffer Layer of $Sb_2S_3$

The next problem to overcome was getting SbSI to form on the surface of the substrate. SbSI does not grow on bare Platinum because of poor adhesion. The first SbSI films were produced by annealing the Pt-Ta-SiO<sub>2</sub>-Si substrate at 600 °C. This produced hillocks on the substrate and lowered the critical energy needed for SbSI nucleation. Although the hillocks gave a starting point for experimental growth, the hillocks also rendered the films useless for any applications.

A breakthrough occurred with an attempt to use an  $Sb_2S_3$  buffer layer. The idea was to first deposit on the substrate using open-system thermal evaporation, followed by the original growth mechanism in the quartz ampoules.  $Sb_2S_3$  grew very easily on a bare (non-annealed) Pt-Ta-SiO<sub>2</sub>-Si substrate. It also provided nucleation sites for the SbSI growth. It was determined that after the closed-tube SbSI growth, the  $Sb_2S_3$  layer completely reacted with the SbSI to form a continuous SbSI film on the substrate. This method was previously accomplished for the growth of PZT and SrTiO<sub>3</sub> thin films [9][13].

### Pre-annealing

Another step in improving the quality of the films was to optimize the SbSI orientation by annealing the buffer layer (pre-annealing) and by post-deposition annealing. The annealing process was kept under 400 °C so that no hillocks formed on the substrate.

## Characterization of SbSI Thin Films

### Scanning Electron Microscopy (SEM)

The simplest method used to observe the quality of the film was to view them with an SEM. If the SbSI needle crystallites are not present under the SEM, then the film is not stoichiometric. If the needles are present then the density and orientation of the crystallites can be observed. The goal was to produce a film with densely packed needles oriented perpendicular to the substrate.

### Energy Dispersive Spectroscopy (EDS)

Standardless Electron dispersive spectroscopy was performed on the samples in the SEM. EDS analyzes the wavelength and amplitude of radiation given off by the sample and determines its chemical composition. Unfortunately, the standardless EDS is limited by an error range of +/-3%. All samples generated by the closed-tube physical vapor transport method had good stoichiometry (33% of each Sb, S, and I) within the +/- 3% accuracy of the EDS.

### X-Ray Diffraction (XRD)

X-Ray diffraction analysis was used to determine the quality of the film in terms of the primary crystal orientation. Scanning Electron Microscopy was also used to observe the density and alignment of the SbSI crystals. X-Ray diffraction uses Bragg law to determine the orientation of the crystalline structure:

$$n\lambda = 2d \sin \theta \quad (5)$$

where  $\lambda$  is the wavelength of the incident x-ray,  $d$  is the spacing between planes, and  $\theta$  is the angle of the incident radiation. For a given crystal structure, there is an angle that corresponds to the maximum diffracted radiation. The XRD pattern provides a chart showing the orientations present in the sample. The XRD was the primary analytical tool to determine the quality of the film.

### Electrical Characterization

Electrical characterization was performed using the setup shown in Figure 10. Plantinized silicon substrates were used in the electrical characterization experiments. The platinum served as the bottom electrode, and 100 $\mu$ m top-electrodes were deposited by gold sputtering. The sample was placed onto the solid-state temperature controller with a non-conductive thermal grease. The Pentium computer controlled the temperature and sampled the output. The capacitance was calculated with the following formula:

$$C = \frac{V_{dc} \times LI_{sen} \times PA_{sen}}{V_{rms} \times \omega} \quad (6)$$

where  $V_{dc}$  is the output of the lock-in amplifier,  $LI_{sen}$  is the sensitivity of the lock-in amplifier,  $PA_{sen}$  is the pre-amp sensitivity,  $V_{rms}$  is the output of the signal generator, and  $\omega$  is the frequency of the signal. The dielectric permittivity was calculated from the capacitance using equation 4.

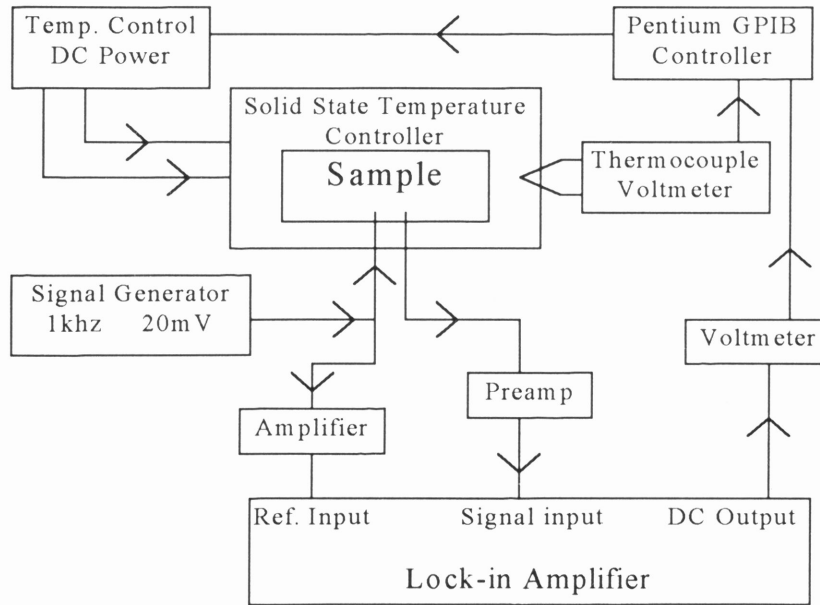


**Figure 10.** Electrical Characterization setup.

### III. RESULTS

#### First Films

The first SbSI films were grown with the annealed platinized silicon substrates and were unusable because of the hillocks present on the substrate. This method would not work for MgO or Al<sub>2</sub>O<sub>3</sub> substrates since they are not affected by high temperature annealing. However, the Pt-Ta-SiO<sub>2</sub>-Si substrate films did show that it was possible to grow stoichiometric SbSI films without complicated post-annealing procedures. The closed-tube growth mechanism was a viable method for correcting the problem of different vapor pressures of S, Sb, and I. Figure 11 and 12 show an SEM micrograph and an XRD pattern for a film grown on the annealed substrate. The SbSI needles in this film were randomly oriented. The random orientation of the needles reduced the density of the film and caused voids. XRD peaks labeled with an asterisk are caused by the substrate

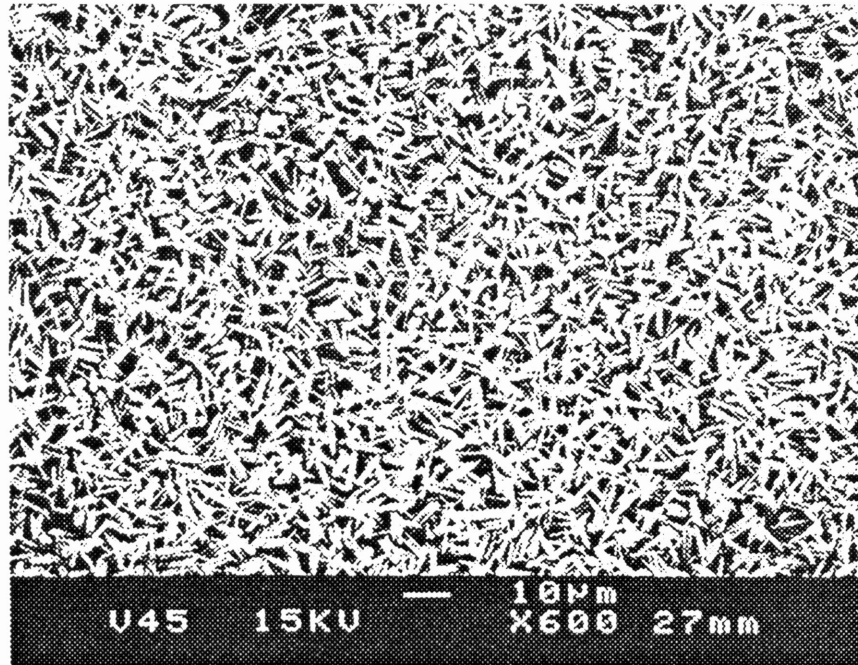


**Figure 11.** SEM of an SbSI film grown on an annealed platinized silicon substrate.



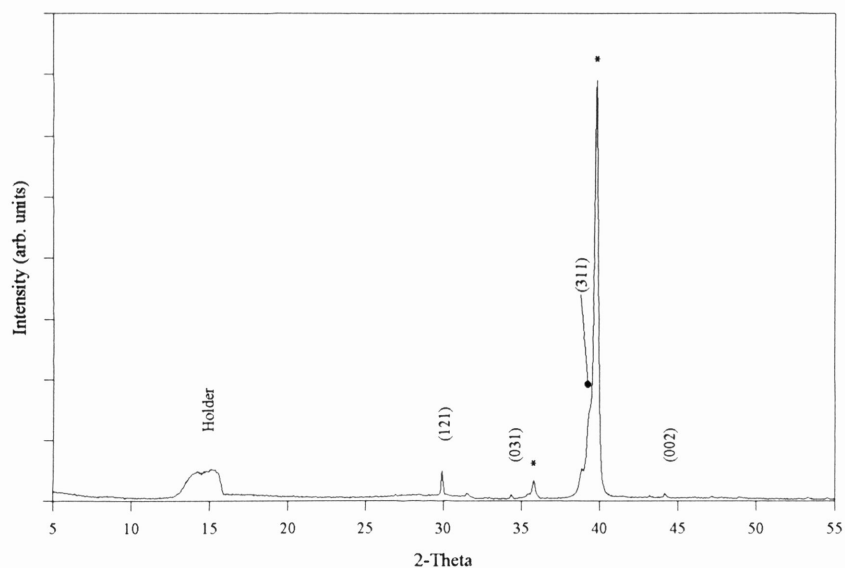


**Figure 12.** XRD of an SbSI film grown on an annealed platinized silicon substrate.

and should be ignored. The XRD shows a preferential (311) crystal orientation, as also found by Mansingh [3]. This orientation is not advantageous for either computer memory or infra-red detection applications. The highest dielectric constant is determined for film specimens with the (002) orientation.

### Buffer Layers

An  $Sb_2S_3$  buffer layer was used to promote SbSI growth on an un-annealed platinized silicon substrate. There are not complications with different vapor pressures of S and Sb, so the sulfide was deposited with an open evaporation method. The buffer layer also allowed growth on both MgO and  $Al_2O_3$  substrates. Figure 13 and 14 show an SEM and XRD of a film grown with a sulfide buffer layer. The buffer layer also improved the

density of the SbSI needles, but the needle orientation was still random. The primary crystal orientation was (121), also seen by Mansingh [3] on annealed SbSI films.

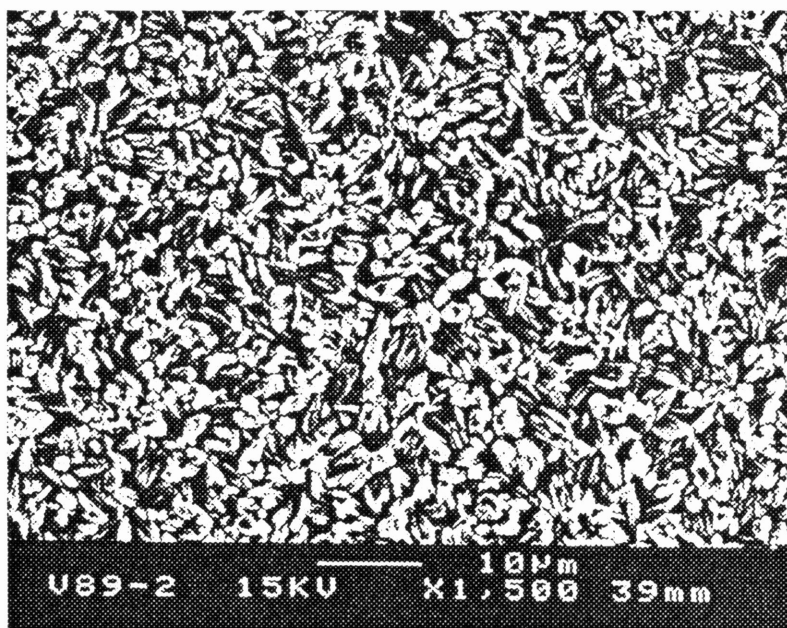


**Figure 13.** SEM of an SbSI film grown with a sulfide buffer layer.

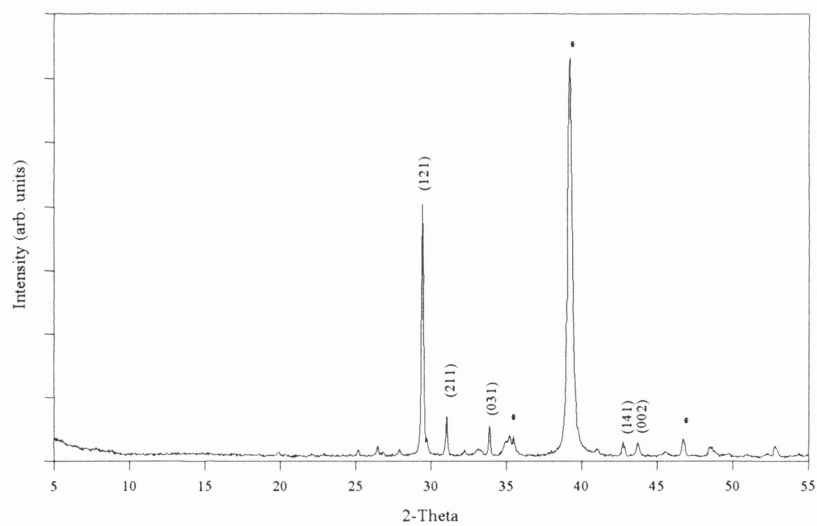


**Figure 14.** XRD of an SbSI film grown with a sulfide buffer layer.

## Pre-annealing

Since the sulfide layer provided nucleation sites for the growth of the SbSI, it was hoped that by pre-annealing the buffer layer, the SbSI orientation could be controlled. A series of experiments showed that a pre-anneal at 250 °C for 5 minutes produced the best (002) oriented films with the SbSI needles perpendicular to the substrate (Figure 15).

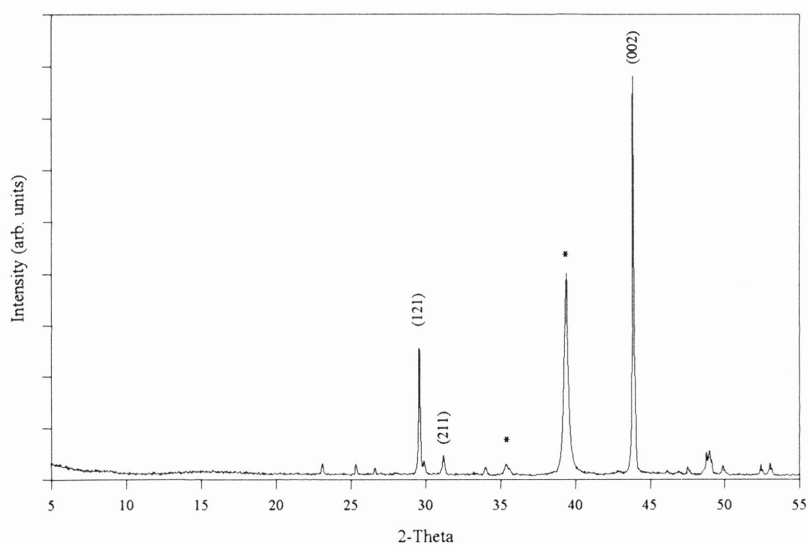


**Figure 15.** XRD of an SbSI film grown with a 250°C pre-annealed sulfide buffer layer.

A 300 °C pre-anneal for 10 minutes produced films with a (220) orientation with SbSI needles parallel to the substrate (Figure 16). The sulfide buffer layer and pre-annealing have provided a method to fully control the orientation of the SbSI crystallites in the thin films.

Electrical characterization has been limited due to the lack of proper probing equipment. Micro-probes were ordered and recently arrived. Full electrical characterization is currently being conducted.

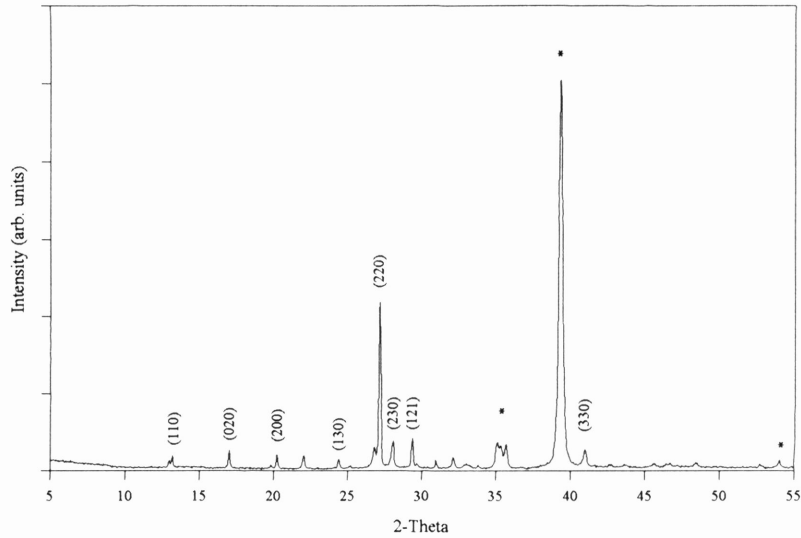


**Figure 16.** XRD of an SbSI film grown with a 300°C pre-annealed sulfide buffer layer.

#### IV. WORK TO BE COMPLETED

Extensive electrical characterization must be performed on the films to determine if they might meet the high dielectric constant needed for computer memory applications. Optical characterization also needs to be performed to determine if the films might be used in infrared detectors. The estimate of the film thickness is  $3\mu\text{m}$ , but the exact film thickness must be determined. Computer memory applications will require the film thickness to be reduced to  $0.2\mu\text{m}$  [6]. This might be accomplished by lowering the growth time and reducing the SbSI grain size. Experiments to improve crystal orientation and dipole alignment are being pursued. These include SbSI growth in the presence of an electric or magnetic field. Also, mis-orientations present in the films need to be reduced. A new furnace with reduced temperature fluctuations has been recently acquired and will hopefully solve these problems.

## Acknowledgments

I would like to thank Narayan Solayappan, a Ph.D. student in the Center for Electronic Materials, Devices, and Systems (CEMDAS), for his guidance, knowledge, patience, and generosity. His constant help and teaching about research methodology was valuable to my education and experience and allowed me to develop motivation and dedication for doing research. Without his personal interest and encouragement it would have been extremely difficult for me to gain a deep insight in the subject matter of this research topic. I would also like to thank Dr. R. K. Pandey for his kindness, guidance, and advice. Lastly, I would like to thank the University Fellows program and Dr. Susanna Finnell for providing a research opportunity that has broadened my mind and opened many opportunities for graduate study.

## References Cited

- [1] B. K. Moon and H. Ishiwara, *Jpn. J. of Appl. Phys.*, Vol. 33, No. 3A, pp. 1472-1477, 1994.
- [2] M. Yoshida et al., *Jpn. J. of Appl. Phys.*, Vol. 12, pp. 1699-1705, 1973.
- [3] A. Mansingh and T. S. Rao, *J. Appl. Phys.*, Vol. 58, pp. 3530-3535, 1985.
- [4] N. Solayappan, class report.
- [5] J.S. Lee et al., *Jpn. J. of Appl. Phys.*, Vol. 33, No. 1A, pp. 260-265, 1994.
- [6] L. H. Parker and A. F. Tasch, *IEEE Cir. and Dev.*, pp.17-26, 1990.

## Works Consulted

- [1] "An American National Standard: IEEE Standard Definitions of Primary Ferroelectric Terms." 1986.
- [2] D. W. Bondurant and F. P. Gnadinger, *IEEE Spectrum*, Vol 26, pp. 30-33, 1989.
- [3] D. W. Bondurant et al., *Proc. of IEEE 1991 Nat. Aero. and Elec Conf. 1991*, Vol. 1, pp. 30-33, 1989.
- [4] J. C. Burfoot and G. W. Taylor, *Polar Dielectrics and Their Applications*, U. of California, 1979.
- [5] L. E. Cross et al., application for patent.
- [6] D. E. Fisch et al., *28th Ann. Proc. on Rel. Phys. 1990*, pp. 237-242, 1990.
- [7] W. A. Geideman, *IEEE Trans. on Ultra., Ferro., and Freq. Control*, Vol. 38, pp. 704-711, 1991.
- [8] C. Hu ed., *Nonvolatile Semiconductor Memories: Technologies, Design, and Applications*, 1991.
- [9] G. C. Messenger and F. N. Coppage, *IEEE Trans. on Nuc. Sc.*, Vol. 35, pp. 1461-1466, 1988.
- [10] S. Middelhoek et al., *Physics of Computer Memory Devices*, 1976.
- [11] J. F. Scott et al., *IEEE 1989 Ultra. Symp. Proc.*, Vol. 1, pp. 299-308, 1989.
- [12] N. Solayappan et al., to be submitted to *J. of Mat. Res.*